UNCLASSIFIED

FIRST INTERIM REPORT

ON

STUDY OF HF FREQUENCIES FOR EXO- AND ENDO-IONOSPHERIC COMMUNICATIONS.

PERIOD COVERED:

MARCH 28, 1962

JUNE 28, 1962

AF CONTRACT AF 33 (657) -7791

THE RESEARCH REPORTED IN THIS DOCUMENT HAS BEEN MADE POSSIBLE THROUGH SUPPORT AND SPONSORSHIP EXTENDED BY THE ELECTROMAGNETIC WARFARE AND COMMUNICATIONS LABORATORY OF THE WRIGHT DEVELOPMENT DIVISION, UNDER CONTRACT NO. AF 33 (657) – 7791. IT IS PUBLISHED FOR TECHNICAL INFORMATION ONLY AND DOES NOT NECESSARILY REPRESENT RECOMMENDATIONS OR CONCLUSIONS OF THE SPONSORING AGENCY.

RAYTHEON COMPANY
MISSILE AND SPACE DIVISION
ADVANCED DEVELOPMENT LABORATORY
BEDFORD, MASSACHUSETTS.

UNCLASSIFIED

ABSTRACT

This Interim Report furnishes preliminary results on an analysis of HF ionospheric propagation, which has the major aim of searching for wave-guidance modes in the upper ionosphere, across the F_2 layer, and below it.
In order to perform this search a Hamiltonian ray tracing method has been developed to include the effect of the earth magnetic field, of the collisional frequency, of various models of ionospheric irregularities and discontinuities, upon the HF propagation.
The search for wave-guidance modes has been oriented toward a possible use of these modes in satellite-to-satellite, satellite-to-ground communications beyond line of sight. Possibility to apply some of these modes to global communications has been also analyzed.
A computer program which performs the Hamiltonian ray-tracing allows the calculation of the main parameters of the rays considered: total path losses, bandwidth available, e.m. wave polarization, multipath structure are among the computed ray's characteristics.

TABLE OF CONTENT

1.0 INTRODUCTION

1.1 General

Since the early practice of HF ionospheric propagation with both the terminals of the links located on the earth's surface, "circumferential transits", as are called very long-range propagation modes involving one or more paths around the earth, have been observed.

The related path losses, even over exceedingly large distances, have been generally found very low; this finding has oriented various investigators to explain these modes on the basis of some sort of ionospheric channeling, instead of on the basis of just multihop path propagation between the ionosphere and the earth's surface.

Gerson (1961) gives a recent review of the investigations performed in this domain, going back to the early work of Eckersley and Marconi; he illustrates the various types of mechanisms which have been postulated to explain the circumferential transits, including M-type reflections, migratory reflections and ductings.

All these mechanisms need to explain the launching of the wave in the duct and the extraction of the same from it, by virtue of some local layer peculiarity (tilts, scattering irregularities, leakages, holes, refractive discontinuities, etc.) both above the transmitting and the receiving ends of the link.

The combined probability, necessarily low, of fulfilling the injection and extraction requirements has been invoked as the main reason to explain the relative rarity of these modes, which sets very definite limitations to the practicality of their use for long-range reliable communications.

The advent of the artificial satellite has revived the interest in these long-range propagation modes, inasmuch, if an ionospheric duct does exist, the HF transmitter, e.g., can be located now inside it and therefore minimized injection difficulties result. Only for the extraction of the wave from the duct, a local layer peculiarity is still needed, above the receiving end of the link.

The probability of achieving circumferential transits is higher now than in the situations previously considered (where both the terminals are located on the earth's surface); although no fully established evidence of this increased probability exists yet, owing to the rather small volume of data collected up until

now for this specific situation, extreme distances have been, however, repeatedly reported in HF links at 20 mc/s and 40 mc/s with a satellite-borne low-power transmitting end, and a receiving station in the earth's surface. The literature provides various information on these findings (Wells, 1958; Woyk, 1959; Isted 1959), which strengthen the hypothesis that some ionospheric channeling is involved.

* * *

The basic motivation to start the research work reported herein has been the reasoning that, if some ionospheric channeling does exist, one effective way of using it for long-range reliable communications consists in placing both the transmitting and the receiving ends of the link in the duct, to minimize consequently both the wave injection and extraction difficulties. This can be done by using satellite-borne HF equipment, with nondirective antennas and low-power emissions.

The title of our program has been chosen in view of the fact that in our search for long-range propagation modes we have investigated the existence of these modes both above the ionospheric F_2 layer (exo-ionospheric cases), and underneath and across the same (endo-ionospheric cases). In the exo-ionospheric case (ducting located above the F_2 layer) a satellite communication system can conceivably use the wave guidance available, with both terminals of the link orbiting at high altitude above the layer of maximum electron density; for this case the ionosphere provides some isolation between the link itself and the earth's surface, when the link's frequency is low enough with respect to $F_{2\,\text{maximum}}$ critical frequency. In the endo-ionospheric case (wave guidance provided by ducting across and underneath the F_2 layer) a satellite system can use the duct, with one of the terminals above and the other below, or both below the ionospheric layer of maximum electron density.

For this last situation (ductings located underneath the F_2 layer), systems other than satellite communication networks can conceivably utilize this ionospheric channeling. Makrakis (1960) has, for instance, suggested the use of a particular one of them in a ground-based global communication system where the problem of the wave injection and extraction in and from the ducting is solved by the use of artificial scattering centers located one above the transmitting and one above the receiving end of the link.

In addition to the search for the existence of HF wave guidance modes in the ionosphere, we are performing in our study the analysis of their characteristics which are of importance for their use in long-range reliable communications, like the total path losses, the frequency dispersion and the multipath structure (which directly affect the data rate achievable in the link), the e.m. wave polarization, the degree of sensitivity of these modes to refraction and absorption effects of large-scale irregularities and discontinuities, the link's expected $S/_N$ ratio.

1.2 Conceivable System Applications of Exo- and Endo-Ionospheric Long-Range HF Propagation Modes

The work performed in the present contract provides analytical evidence of the existence, and limitations thereof, of long-range HF modes in the ionosphere, and furnishes an evaluation of their properties.

An experimental verification of the existence of these modes through the use of satellite payloads as mobile terminals of a propagation survey link seems the most advisable step to perform next; if the experiment would indeed prove their existence, various would be the communication schemes which could utilize these modes.

In fact global range, real time communications between earth stations and aerospace vehicles, including vehicle-to-vehicle communications, is a requirement. Possible vehicles participating in such links include early-warning satellites, manned reconnaissance satellites, boost-glide vehicles.

Present techniques for global communications include LF, HF, and multiple point-to-point relay with attendant difficulties in propagation outages and system complexity.

Passive and active relay satellites are in development for future application to the general communication relay problem. Devices of both categories have finite performance limitations, and are expensive in terms of development and launching into orbit or on station.

The HF propagation modes studied within the present contract may constitute an interesting way of approaching both the problem of global communications and the one of space vehicle-to-vehicle and vehicle-to-ground links. As an example of a conceivable system based on the use of these modes, we consider a satellite communication link.

The use of low RF power level at the transmitting end, the possibility of avoiding any satellite stabilization problem because of the use of nondirective antennas, and the low number of satellites sufficient for a global coverage are the interesting features of such a link. The limited bandwidth available may discourage its application to high data rate communication channels.

In Figure 1 is illustrated a highly idealized scheme for this satellite-to-satellite communication link enabling global coverage; the link uses exo- or endo-ionospheric long-range, HF propagation modes. If the link just performs satellite-to-satellite communication, the scheme is self-explanatory. If the link is used to allow communications between Ground Station 1 and Ground Station 2, the scheme may work as follows. Both the terminals of the HF ionospheric link are connected with the earth's surface by means of line-of-sight UHF links for which the ionosphere is fully transparent.

Satellites 1 and 2 are identical (they are among about 10 satellites orbiting, say, at about 3000 Km of altitude). Each satellite carries an HF transreceiver, with a certain number of preset frequencies available in the HF band and an identical UHF T_x/R_c.

Suppose that Satellite 1 is within the reach of Ground Station 1, and Satellite 2 of Station 2. Through the two-way UHF link, Station 1 chooses in the satellite the HF transmitting frequency allocated to the station itself and starts to broadcast in HF its message; Station 1 chooses as a receiving frequency the one allocated to the emission of Station 2. This last station proceeds in a similar way, by choosing in the satellite its own allocated frequency for the emission and the receiving frequency corresponding the emission of Station 1. Under the assumption that a ducting is available to the HF propagation beyond the line-of-sight between Satellites 1 and 2, a link is established between Ground Stations 1 and 2.

When one of the satellites gets out from the coverage of the ground station which utilized it, it stops to radiate both in HF and UHF and becomes "available" for another ground station.

The number of the satellites has to be chosen in such a way that one of them is always within the coverage of a ground station for a very high percentage of the time. A calculation we did has shown that 10 satellites, orbiting at 3000 Km of altitude, would assure the good coverage of a large number of ground stations. The link compares favorably with the HF ionospheric communication which could be established between Ground Stations 1 and 2 in the traditional ways.

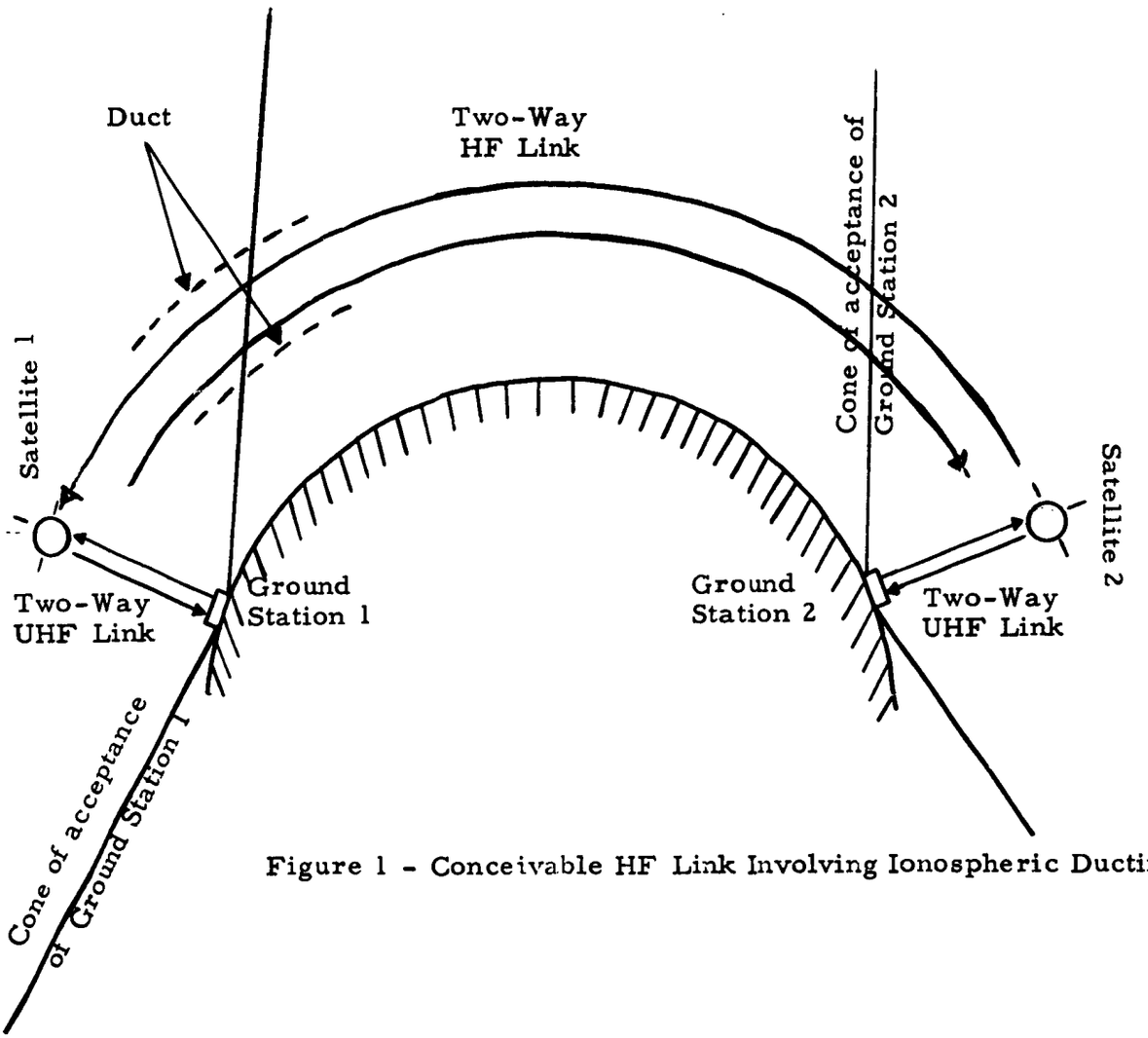

Figure 1 - Conceivable HF Link Involving Ionospheric Ducting

2.0 THE HAMILTONIAN RAY TRACING, AS AN ANALYTICAL TOOL FOR THE INVESTIGATION OF HF IONOSPHERIC PROPAGATION

2.1 General

The analytical tool utilized in this program for the investigation of HF long-range propagation modes is the Hamiltonian ray-tracing developed for ionospheric calculation by J. Haselgrove (1955). The method gives the equations governing the ray path in an anisotropic medium in a form which is suitable for integration by standard numerical methods using a digital computer. The equations are derived from the Fermat principle of stationary time.

In an anisotropic medium, the energy associated with e.m. waves does not in general travel in the direction of the wave normal, even in the case of plane waves, but in a different direction called ray direction. In an inhomogeneous anisotropic medium, like the ionosphere in presence of the earth's magnetic field, the energy follows a curved path, called the ray path. The differential equations which determine the ray path used in this program, were given by Hamilton in 1837 in the Third Supplement to his treatise on Geometrical Optics for a General Anisotropic Medium (Hamilton 1931). Haselgrove has derived these equations in spherical coordinates suitable for treatment of three-dimensional ionospheric problems.

2.2 The Basic Equations

The equations are as follows:

$$\dot{r} = \frac{1}{\mu^2}\left[y_1 - \mu\frac{\partial\mu}{\partial y_1}\right] ; \tag{1}$$

$$\dot{\theta} = \frac{1}{\mu^2 r}\left[y_2 - \mu\frac{\partial\mu}{\partial y_2}\right] ; \tag{2}$$

$$\dot{\phi} = \frac{1}{\mu^2 r\sin\theta}\left[y_3 - \mu\frac{\partial\mu}{\partial y_3}\right] ; \tag{3}$$

$$\dot{y}_1 = \frac{1}{\mu}\frac{\partial\mu}{\partial r} + \dot{\theta}y_2 + \dot{\phi}y_3\sin\theta ; \tag{4}$$

$$\dot{y}_2 = \frac{1}{r}\left[\frac{1}{\mu}\frac{\partial\mu}{\partial\theta} - \dot{r}y_2 + \dot{\phi}y_3 r\cos\theta\right] ; \tag{5}$$

$$\dot{y}_3 = \frac{1}{r\sin\theta}\left[\frac{1}{\mu}\frac{\partial\mu}{\partial\phi} - \dot{r}y_3\sin\theta - \dot{\theta}y_3 r\cos\theta\right] . \tag{6}$$

The quantities in equations (1) through (6) are defined as follows: r, θ, ϕ are the spherical coordinates of a point in the earth's ionosphere; y_1, y_2, y_3 represent the components of the wave normal with respect to a Cartesian system whose origin is placed at r, θ, ϕ. This system is illustrated in Figure 2. The y_1 direction is along r; y_2 along θ; and y_3 along ϕ. The system is chosen to be right-handed and orthogonal; $\dot{r}$, $\dot{\theta}$, etc., are the derivatives of these variables with respect to time. The method is fully three-dimensional and therefore can treat rays both contained and not contained in the great-circle plane of the HF link.

The phase refractive index, μ, is given explicitly by a form of the Appleton-Hartree formula (when collisions between electrons and air molecules or positive ions are neglected):

$$\mu^2 = 1 - \frac{\dfrac{N(r,\theta,\phi)}{1.24 \times 10^4 f^2}}{1 - M \pm \sqrt{M^2 + \dfrac{f_H^2}{f^2} \cos^2 \psi_{MG}}} \qquad (7)$$

where

f = frequency of radiation in Mc/s;

$N(r, \theta, \phi)$ = number of electrons/cm^3 (the electron density is, in general, dependent upon the position in the ionosphere as well as the height of the point under consideration).

f_H = the gyrofrequency in Mc/sec and M is given by

$$M = \frac{\dfrac{1}{2}\left[\dfrac{f_H}{f} \sin \psi_{MG}\right]^2}{1 - \dfrac{N(r,\theta,\phi)}{1.24 \times 10^4 f^2}}$$

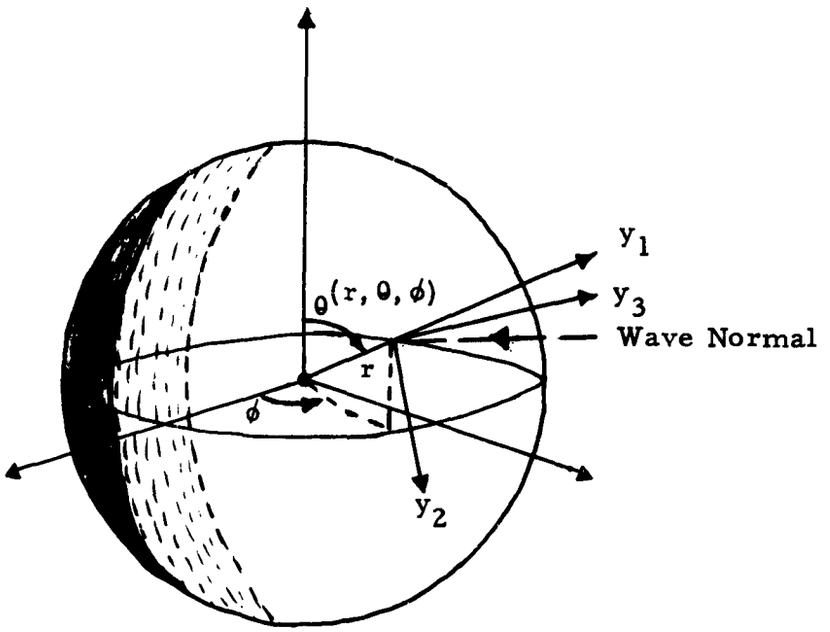

Figure 2 - System of Reference

(ψ_{MG} = the angle between the wave normal and the earth's magnetic field,) If the field is taken to be a dipole in nature and if the polar axis of the spherical coordinate system coincides with the dipole axis, as we do here, then

$$\cos\psi_{MG} = \frac{y_1 \cos\theta + \frac{1}{2} y_2 \sin\theta}{\left[y_1^2 + y_2^2 + y_3^2\right]^{1/2} \left[\cos^2\theta + \frac{1}{4}\sin^2\theta\right]^{1/2}}.$$

When collision between electrons and air molecules or ions is not negligible, the refraction index M becomes a complex number of which the real part plays the same role as μ previously considered, while the coefficient of the imaginary part is the absorption coefficient of the wave.

We have

$$M = \mu - j\frac{ck}{2\pi f} = \left(1 - \frac{X}{1 - jZ - \frac{\frac{1}{2} Y^2 \sin^2\psi}{1-X-jZ} \pm \left[\left(\frac{\frac{1}{2} Y^2 \sin^2\psi}{1-X-jZ}\right)^2 + Y^2\cos^2\psi\right]^{\frac{1}{2}}}\right)^{\frac{1}{2}}$$

where

c = velocity of the light in vacuo = 300×10^6 m/sec

k = absorption coefficient

f = frequency of the e.m. wave

$$X = \frac{N(r, \theta, \phi)}{1.24 \times 10^4 \times f^2}$$

$$Y = \frac{f_H(r, \theta)}{f}, \quad f_H = \frac{0.9\, a^3}{r^3} \sqrt{1 + 3\cos^2\theta}$$

$$Z = \frac{\nu(r, \theta, \phi)}{2\pi f}.$$

If we disregard collision, $\nu = 0$, $Z = 0$ and we go back to the known expression:

$$M^2 = \mu^2 = 1 - \frac{X}{1 - \frac{\frac{1}{2} Y^2 \sin^2\psi}{1 - X} \pm \left[\left(\frac{\frac{1}{2} Y^2 \sin^2\psi}{1 - X}\right)^2 + Y^2 \cos^2\psi\right]^{1/2}}$$

$$= 1 - \frac{\frac{N(r, \theta, \phi)}{1.24 \times 10^4 \times f^2}}{1 - M \pm \sqrt{M^2 + \frac{f_H^2}{f^2} \cos^2\psi}}.$$

In order to organize the computation, we call,

$$A - jB = 1 - jZ - (a + jb) \pm \left[(a + jb)^2 + y^2 \cos^2\psi\right]^{1/2}$$

where

$$a + jb = \frac{\frac{1}{2} y^2 \sin^2 \psi}{1 - x - jZ}$$

$$a + jb = \frac{\frac{1}{2} y^2 \sin^2 \psi (1 - x + jZ)}{(1 - x)^2 + Z^2} = \frac{\frac{1}{2} y^2 \sin^2 \psi (1 - x)}{(1 - x)^2 + Z^2} + j \frac{\frac{1}{2} y^2 \sin^2 \psi Z}{(1 - x)^2 + Z^2}$$

and

$$\mu^2 = \sqrt{E^2 + F^2} + E \qquad a = \frac{\frac{1}{2} y^2 \sin^2 \psi (1 - x)}{(1 - x)^2 + Z^2}$$

$$\frac{ck}{2\pi f} = \sqrt{\sqrt{E^2 + F^2} - E} \qquad b = \frac{\frac{1}{2} y^2 \sin^2 \psi - Z}{(1 - x)^2 + Z^2}$$

where

$$E = \frac{1}{2} - \frac{Ax}{2 (A^2 + B^2)}$$

$$F = \frac{Bx}{2 (A^2 + B^2)} .$$

In developing the computations, we have:

$$A - j B = 1 - a \pm \mathrm{Re} \left\{ \left[(a + jb)^2 + y^2 \cos^2 \psi \right]^{1/2} \right\} - jZ - jb \pm \mathrm{Im} \left\{ \left[(a + jb)^2 + y^2 \cos^2 \psi \right]^{1/2} \right\}$$

$$= 1 - a \pm W - j \left(Z + b \mp \frac{V}{2 W} \right)$$

$$U + jV = (a + jb)^2 + y^2 \cos^2 \psi = a^2 - b^2 + j\, 2ab + y^2 \cos^2 \psi$$

where

$$U = a^2 - b^2 + y^2\cos^2\psi = \left[\frac{\frac{1}{2}y^2\sin^2\psi\,(1-x)}{(1-x)^2+Z^2}\right]^2 - \left[\frac{\frac{1}{2}y^2\sin^2\psi\cdot Z}{(1-x)^2+Z^2}\right]^2 + y^2\cos^2\psi \simeq \left[\frac{\frac{1}{2}\frac{f_H^2}{f^2}\sin^2\psi\left(1-\frac{N}{1.24\cdot 10^4\cdot f^2}\right)}{\left(1-\frac{N}{1.24\cdot 10^4\cdot f^2}\right)^2+\left(\frac{\nu}{2\pi f}\right)^2}\right]^2 - \left[\frac{\frac{1}{2}\frac{f_H^2}{f^2}\sin^2\psi\cdot\left(\frac{\nu}{2\pi f}\right)}{\left(1-\frac{N}{1.24\cdot 10^4\cdot f^2}\right)^2+\left(\frac{\nu}{2\pi f}\right)^2}\right]^2 + \frac{f_H^2}{f^2}\cos^2\psi$$

$$V = 2ab = 2\,\frac{\frac{1}{2}y^2\sin^2\psi\,(1-x)}{(1-x)^2+Z^2}\cdot\frac{\frac{1}{2}y^2\sin^2\psi\cdot Z}{(1-x)^2+Z^2} = \frac{1}{2}\,\frac{\left(\frac{f_H}{f}\right)^4\sin^4\psi\left(1-\frac{N}{1.24\cdot 10^4\cdot f^2}\right)\frac{\nu}{2\pi f}}{\left[\left(1-\frac{N}{1.24\cdot 10^4\cdot f^2}\right)^2+\left(\frac{\nu}{2\pi f}\right)^2\right]^2}$$

$$2W^2 = U + (U^2+V^2)^{1/2} \qquad W = \left\{\frac{1}{2}\left[U+(U^2+V^2)^{1/2}\right]\right\}^{1/2}$$

$$A = 1 - a \pm W = 1 - \frac{\frac{1}{2}\left(\frac{f_H}{f}\right)^2\sin^2\psi\,(1-x)}{(1-x)^2+Z^2} \pm \left\{\frac{1}{2}\left[U+(U^2+V^2)^{1/2}\right]\right\}^{1/2} = 1 - \frac{\frac{1}{2}\left(\frac{f_H}{f}\right)^2\sin^2\psi\left(1-\frac{N}{1.24\cdot 10^4\cdot f^2}\right)}{\left(1-\frac{N}{1.24\cdot 10^4\cdot f^2}\right)^2+\left(\frac{\nu}{2\pi f}\right)^2} \pm \left\{\frac{1}{2}\left[U+(U^2+V^2)^{1/2}\right]\right\}^{1/2}$$

$$B = Z + B \mp \frac{V}{2W} = Z + \frac{\frac{1}{2}\left(\frac{f_H}{f}\right)^2\sin^2\psi\cdot Z}{(1-x)^2+Z^2} \mp \frac{V}{2\left\{\frac{1}{2}\left[U+(U^2+V^2)^{1/2}\right]\right\}^{1/2}} = \frac{\nu}{2\pi f} + \frac{\frac{1}{2}\left(\frac{f_H}{f}\right)^2\sin^2\psi\cdot\frac{\nu}{2\pi f}}{\left(1-\frac{N}{1.24\times 10^4\times f^2}\right)^2+\left(\frac{\nu}{2\pi f}\right)^2} \mp \frac{V}{2\left\{\frac{1}{2}\left[U+(U^2+V^2)^{1/2}\right]\right\}^{1/2}}$$

Finally,

$$\mu^2 = (E^2 + F^2)^{1/2} + E = \left\{\left[\frac{1}{2} - \frac{Ax}{2(A^2 + B^2)}\right]^2 + \left[\frac{Bx}{2(A^2 + B^2)}\right]^2\right\}^{1/2} + \frac{1}{2} - \frac{Ax}{2(A^2 + B^2)} =$$

$$= \left\{\left[\frac{1}{2} - \frac{A\dfrac{N}{1.24 \times 10^4 f^2}}{2(A^2 + B^2)}\right]^2 + \left[\frac{B\dfrac{N}{1.24 \times 10^4 \times f^2}}{2(A^2 + B^2)}\right]^2\right\}^{1/2} + \frac{1}{2} - \frac{A\dfrac{N}{1.24 \times 10^4 xf^2}}{2(A^2 + B^2)} .$$

The expression has been written for the IBM-704 computer with subroutines for

N, as function of r, θ, ϕ

$\cos \psi$, as function of y_1, y_2, y_3, θ, ϕ, r

f_H, as function of r, θ, ϕ

ν, as function of r, θ, ϕ

2.3 Mathematical Techniques and Computer Program

The method chosen for numerical integration of equations (1) through (6) is the fourth-order Runge-Kutta method. The advantage of this method lies in the fact that we need only know the values of the variables r, θ, ϕ, y_1, y_2, y_3 at $t = t_o$. In other words, only one set of initial conditions is needed with which to beging the integration. A detailed analysis of the method can be found in Hildebrand (1956), Bateman, Bennet, and Milne (1956) and Balston and Wilf (1960).

We assign the position, and we assume the direction of the ray and the wave normal initially coincident. The program for solution of the differential equations (1) through (6) is written in FORTRAN.

Numerical solutions of the equations follow from an application of the Runge-Kutta method. The initial conditions and the frequency are read into the machine. Subroutines for electron density profiles and the necessary derivatives are interchangeable for various ionospheric models. Both ordinary and extra-ordinary ray paths can be computed. At each integration step the calculated values of r, θ, ϕ are printed out. Calculation time for ray paths of 10^4 km is approximately 1.5 minutes on the IBM-704 computer.

To minimize the accumulation of truncation and round-off errors, a double precision arithmetic has been utilized, with provisions for integration with fixed and variable step sizes.

2.4 The Models Adopted

The ray tracing utilized in this program requires the adoption of three models: one for the earth's magnetic field, one for the ionospheric electron density, and one for the ionospheric collisional frequency.

For the earth's magnetic field a three-dimensional, spherically symmetric dipolar model has been adopted, as already told, with the dipole axis coincident with the polar axis of the spherical coordinate system we have assumed.

At a given point (r, θ), the field is given by

$$H = H_o \left(\frac{a}{r}\right)^3 \sqrt{1 + 3\cos^2\theta}$$

where

H_o is the field on the earth's surface at the magnetic equator,

and

a is the radius of the earth.

For the three-dimensional electron density model $N(r, \theta, \phi)$ we assumed a spherically symmetric profile, the cross-section of which, in the plane $N(r)$, is indicated in Figure 3. For the three-dimensional collision frequency model $\nu(r, \theta, \phi)$, we assumed a spherically symmetric profile, the cross section of which, in the plane $\nu(r)$, is shown in Figure 4. These two last models have been introduced in the computation through a curve fitting, which consisted in deriving analytical expressions able to fit the chosen profiles. Particular attention has been paid, when a profile has been fitted with more than one branch, to the continuity of the functions themselves, fitting each branch, at their junction points and to their first and second derivatives. Because a major aim of this work is the search of ducting mechanisms in the ionosphere, every possible care has been taken in preventing spurious ducts that do show up in dependence of discontinuities in the chosen models and in the analytical expressions which fit them.

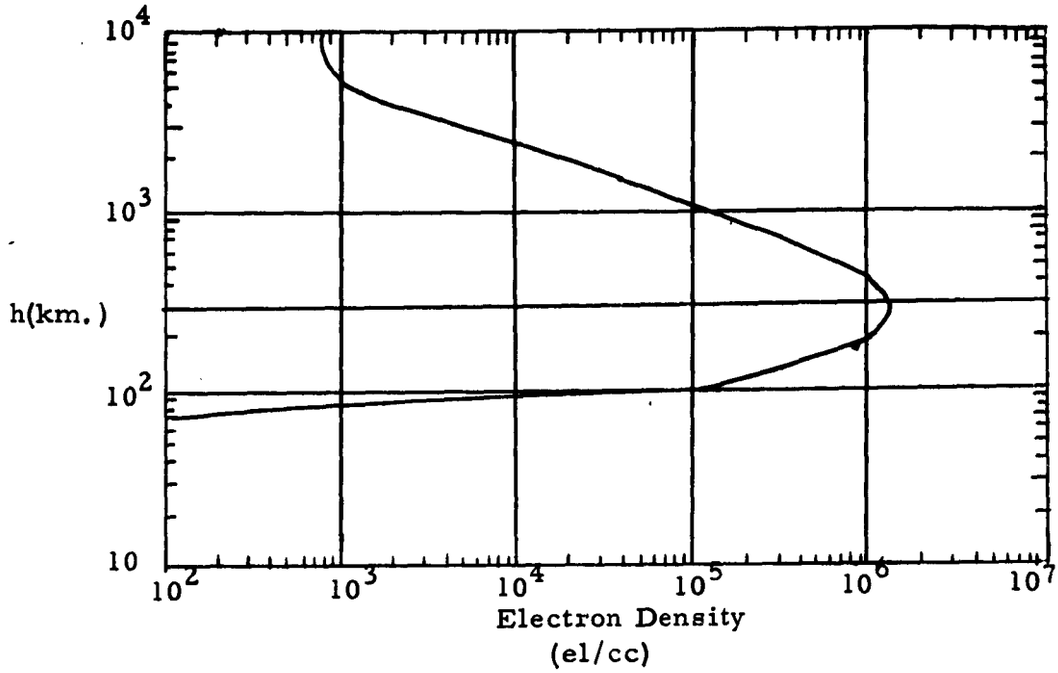

Figure 3 - Electron density profile (average IGY data)

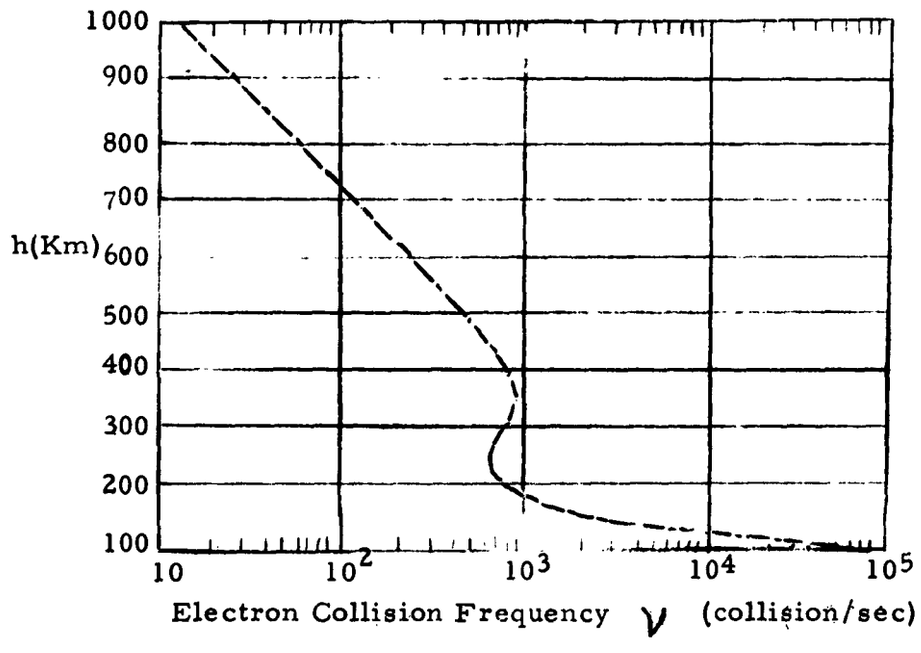

Figure 4 - Electron Collision Frequency ν versus Altitude

3.0 THE SEARCH FOR LONG-RANGE HF PROPAGATION MODES IN THE IONOSPHERE, BETWEEN TERMINALS IMBEDDED IN THE MAGNETO-IONIC MEDIUM

3.1 Case of Terminals Both Located Below the Layer of Maximum Electron Density (F_2 Max.)

A link to be established in this situation can utilize various types of modes, like the one described by Bremmer (1949), Woyk (1959), Rydbeck (1944) and reviewed by Makrakis (1960).

Besides the obvious multihop mode, bound by the ionosphere and the earth's surface, other modes have been investigated, associated with rays which graze the earth's surface or with rays which travel near the ceiling of the ionosphere, and are composed by curved and straight segments inasmuch as they move up and down from the lower ionosphere to the upper atmosphere and vice versa. (When the ray travels the atmosphere it goes straight and when in the ionosphere, proceeds curved.)

Makrakis has postulated another mechanism whereby the lower ionosphere behaves as a generalized Maxwell lens and rays at frequencies around 40 mc/s can travel around the earth without leaving the ionosphere itself. Grossi, Strom and Strom (1961) have postulated an ionospheric Luneberg lens mechanism as to be able to possibly focus cosmic noise waves. Makrakis' duct for 40 mc/s extends about 50 Km above and below 200 Km. His interest is in utilizing this duct for ground station-to-ground station communication and he points out the need of artificial scattering centers to perform injection and extraction of the wave from the duct.

An HF spacecraft-to-spacecraft link, however, could very profitably utilize this duct. At lower frequencies the modes degenerate in the ones previously cited and again the ray shows straight segments.

We have utilized our ray tracing techniques to check these various modes of propagation and we have found confirmation of all of them. Section 5.0 reports details of the computation we performed. These modes are characterized by low refraction losses and we believe have a very definite practical importance in satellite-to-satellite communications, when the vehicles are below F_2 maximum (350 Km circa).

We note that these findings do not rely upon any relative minimum in the electron density profile curve to justify the presence of ionospheric ducting. We found analytical confirmation of the existence of these modes while computing with the profile of Figure 3 as well as with the usual double-exponential Chapman model.

These modes show up at any orientation of the wave normal with respect to the magnetic field and have a remarkable refractive stability. These modes are not isolated from the earth's surface; a "leakage" of variable amount, function, among other variables, of the relative position of the two terminals, takes place.

3.2 Case of Terminals Located One Above and One Below F_2 Maximum

Rawer (1960) has postulated the existence of HF long-range propagation modes suitable to connect two terminals one above and one below F_2 maximum. The mechanism involved is of "penetrating Pedersen-ray" type, working at frequencies around 25 mc/s; here again the existence of the mode does not rely upon any particular anomaly in the shape of the electron density profile and does exist at any inclination of the wave normal with respect to the earth's magnetic field.

We have already applied our Hamiltonian ray tracing program to this case; computations are presently underway.

3.3 Case of Terminals Both Located Above F_2 Maximum

3.3.1 Wave Guidance Provided by the Upper Ionosphere for Transverse Propagation

The magneto-ionic theory (Ratcliffe, 1959; Budden, 1961) shows that in a medium where transverse propagation takes place, and the frequency utilized is larger than the gyrofrequency ($Y < 1$), the index of refraction behaves as indicated in Figure 5 for the extraordinary ray.

With the collision frequency model of Figure 4, the plot of μ in Figure 5 shows the existence of regions in the upper ionosphere where the extraordinary rays propagating transversally may remain trapped between two surfaces, defined respectively by:

$$X \cong 1 - Y$$
$$X \cong 1 + Y.$$

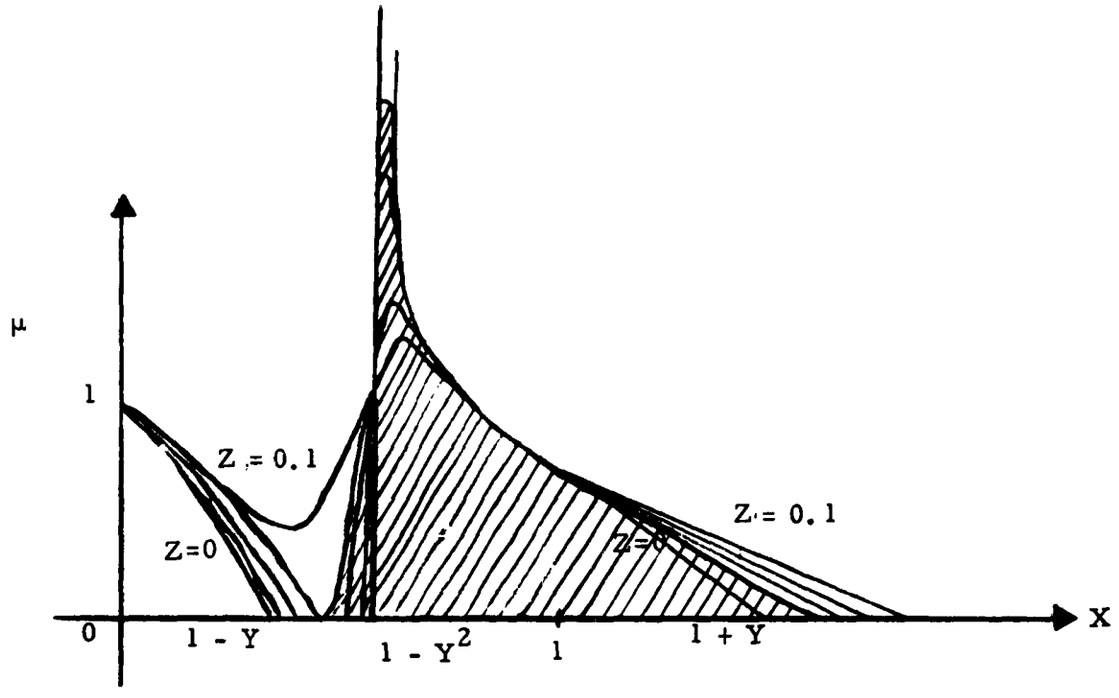

Toward Free Space

Toward F_2 maximum and the Earth's Surface

Figure 5 - Ionospheric index of refraction vs parameter X, for various values of the collision frequency; transversal propagation, $Y < 1$. Extraordinary ray.

Computations are presently underway to locate, for various frequency for for various orientations of the wave normal with respect to the earth's magnetic field, the position of these surfaces and the shape and size of the related ducts.

Because the medium is nonhomogeneous and nonisotropic, the index of refraction is computed by assigning the initial conditions of the e.m. source, corresponding to the position of the transmitting satellite, and by "probing" the surrounding environment with various values of the set (y_1, y_2, y_3).

A pure transverse propagation mode utilizing this mechanism would allow beyond-line-of-sight communications in somewhat restrictive conditions. We are therefore carrying on intensive calculations to check the possibility of extending this type of wave guidance to quasi-transversal propagation and to find the limits of this extension.

Another possibility is represented by the use of frequencies smaller than gyrofrequency ($Y>1$). For these frequencies, the extraordinary rays are characterized by index of refraction slightly larger than one, when $X<1$; therefore rays penetrating the earth's ionosphere from outside may follow the earth's curvature.

Calculations are underway to check this possibility.

3.3.2 Possible Wave Guidance in Case of Longitudinal Propagation

In this case and for frequencies smaller than the gyrofrequency, the ionospheric index of refraction is always larger than one, for any value of X. (Figure 5.). E.M. rays penetrating the ionosphere from outside have a curvature which follows the one of the earth, instead of being refracted toward free space; therefore they provide beyond line-of-sight propagation.

Computations have checked this behavior and we are now investigating the details of the modes and their practicality for HF communication links.

Among the various characteristics we are checking, there is the one related to the possibility of going from purely longitudinal propagation to quasi -longitudinal modes and limits thereof. This effort, combined with the one indicated in paragraph 3.3.1, will tell how general validity have the wave guidance mechanisms we are investigating for the case of terminals both located above F_2 maximum. Our major aim is to check how much overlapping exists

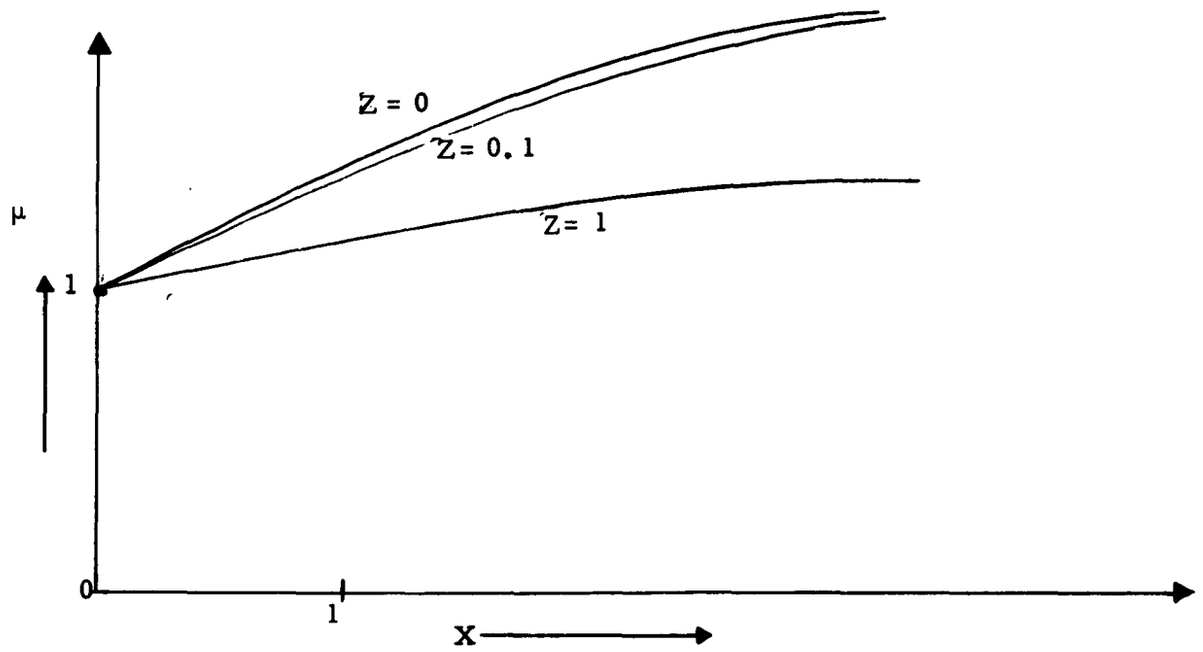

Figure 6 - Ionospheric index of refraction vs parameter X, for various values of the collision frequency. Longitudinal propagation, $Y \gg 1$. Sign minus in the equation $n^2 = 1 - \frac{X}{1 - jZ \pm Y}$

between wave guidance based on quasi-transversal modes and wave guidance based on quasi-longitudinal ones, in order to evaluate the continuity obtainable in HF links between satellites orbiting in the upper ionosphere, in any positional relationship.

3.3.3 Wave Guidance Provided by Field Aligned Ionization Columns and Laminar Structure in the Upper Ionosphere

Experimental data have been collected in the recent past which support the hypothesis of a fibrous and laminar structure of the upper ionosphere.

Obayashi (1959), Booker (1960), Gallet and Utlant (1961) have supported the possibility of longitudinal wave guidance above the F_2 layer by means of ionization columns, or thin sheets aligned along the lines of force of the earth's magnetic field.

This wave guidance applies to HF waves with frequency well above the local critical frequency and the gyrofrequency.

The refractive index along these paths appears to be near to one, the frequency dispersion low, the path losses small.

Extensive experimental programs are presently underway in this country to collect more evidence and formulate a comprehensive theory of the experimental findings.

In our study, we are simulating the ionized column condition by imposing to the electron density profile used in our computer program, a cylindrical disturbance aligned along a magnetic meridian.

The Hamiltonian ray tracing is then applied, the ray path along the column plotted, path losses and dispersions computed.

The final report will provide results of these computations. The data will be of interest for the time that a satellite HF propagation experiment will be performed; they will allow to check whether the explanation of the behavior of the received field intensity needs such ionization enhancement along the lines of force of the magnetic field.

3.3.4 Isolation of the Exoionospheric HF Links from the Earth's Surface

Lee (1958) has provided the foundations for the computations we are performing here, with some modification, as applied to the isolation of

an HF exoionospheric link from the earth's surface. The method works as follows: For a given ground position, assumed as location of an HF receiving station, rays are traced in all directions at the frequency utilized in the exo-ionospheric link, up to the altitudes where the satellite-born transmitter is orbiting. Standard models of $N(r, \theta, \phi)$, magnetic field, $\gamma(r, \theta, \phi)$ are used. For each one of these rays the total path losses are computed (free space plus refraction plus absorption losses).

We discard the rays which have total path losses higher than a specified minimum value. We compute the volume, V_i of the space which contains these rays(this is the "volume of acceptance"); a satellite-borne transmitter contained in V_i will be received by the ground station considered. We find now the ratio between the volume, V_i and the volume, V_o correspondent to the hypothetical conditions of free space. V_o is the volume of a half-sphere, with center at the chosen point on the earth representing the ground station, and radius equal to the range correspondent to the specified value of propagation losses.

The isolation I_r of the transmitter of the HF link from the ground can be defined as

$$I_r = 1 - \frac{V_i}{V_o} .$$

The nature of I_r found in this way is related to a static situation for each of the various models adopted (magnetic field, electron density, collision frequency). To perform a more realistic evaluation about the actual isolation we have to expect, we treat statistically these topic and compute the probability that I_r be greater than a given amount for a certain percentage of the time in the HF links we are considering.

For this we need dynamic models, instead of the three ones mentioned before, for magnetic field, collision frequency, electron density. These models are beyond the scope of the present contract. However, in order to give an example of the computation that can be performed with our method in this respect, we have presently under calculation a case where it is known from the literature, at a given vertical, the probability that the peak of the F_2 layer has an electron content larger than a certain amount for a certain percentage of the time.

From this probability distribution we are computing the probability distribution of V_i, by performing ray tracing with electron density models having N_{max} of various values corresponding to different points in the probability distribution curve considered. Various V_i are computed in this way and a distribution function is built accordingly.

From this one, the probability distribution of I_r is easily derived.

4.0 ANALYSIS OF THE BASIC PARAMETERS WHICH CHARACTERIZE THE LONG-RANGE PROPAGATION MODES STUDIED IN THIS PROGRAM.

4.1 Total path losses.

The losses affecting HF ionospheric rays are of triple origin: 1/Distance^2 law losses, refraction losses, and absorption losses.

A compact formula which expresses the total path losses in a ray can be written as follows:

$$\left.\begin{matrix}\text{Total}\\ \text{path}\\ \text{losses}\end{matrix}\right\} = \frac{\mu_{\text{fin}}}{\mu_{\text{init.}}} \exp\left\{-\int_0^L \frac{\nabla^2 S}{\mu}\, dl\right\} \cdot \exp\left\{-2\int_0^L \alpha_{ab}\, dl\right\}$$

where L is the total lenght of the ray, α_{ab} is related to the absorption coefficient k of the wave by the expression

$$\alpha_{ab} = k \cos\alpha = \frac{2\pi f}{c}\left\{\left[E^2 + F^2\right]^{\frac{1}{2}} - E\right\}^{\frac{1}{2}} \cdot \cos\alpha$$

(with symbols as defined in Section 2) , S is the eikonal function which has the property that the surface S = const is the geometrical wave front.

In the expression of the total path losses the term related to the absorption losses is the last exponential. What remains gives the losses of the law 1/Distance^2 plus the refraction losses: in free space reduces to the sole losses 1/Distance^2.

The calculation of the last exponential is straightforward in the ray tracing. For the computation of the other losses , the method we adopted consists in tracing four rays defining the tube of flux which has the vertex in the source and reaches the region of interest , where

the receiver is supposed located. The computations, of course, take place in the three-dimensional space.

From the average lenght of the rays, the 1/Distance^2 losses are evaluated; for what is concerning the computation of the refraction losses we proceed in this way: The received power is proportional to the radiation intensity of the source (power per unit solid angle) time the solid angle subtended at the vertex by the four rays.

The ratio between this solid angle and the one of the tube of flux which, in a free space situation, would have , at the same (rectified) distance from the source, the same cross-section, gives the value of the refraction losses.

4.2 Amplitude versus Frequency and Phase versus Frequency Response of a Ray.

For a given ray, the amplitude vs. frequency response $A(\omega)$, where $\omega = 2\pi f$, is easily computed with the formula indicated in the previous paragraph, by plotting the total path losses vs. frequency.

This plotting allows the evaluation of the bandwidth available in the ray itself. This element is of importance in establishing techniques able to counteract the effects of the multipath structure of the HF propagation upon the information rate achievable in the links we are considering. By choosing the correspondent value assumed by the index of refraction , we can treat cases of ionosphere with or without magnetic field and/or collision.

The description of the ray response is complete when the phase vs. frequency response is known.

In the following pages we illustrate the avenue we have chosen in evaluating this parameter.

The expression of the phase constant:

$$\beta(\omega) = \frac{2\pi}{\lambda_{iono.}} = \frac{\omega}{c} \mu_{iono.}$$

leads to the basic formulas to be used in this analysis.

By developing $\beta(\omega)$ in Taylor series, we have

$$\beta(\omega) = \beta(\omega_o) + (\omega - \omega_o)\beta'(\omega_o) + \frac{(\omega - \omega_o)^2}{2} \beta''(\omega_o) + \ldots$$

where

ω_o is the carrier frequency

$$\beta'(\omega_o) = \frac{1}{c} \left\{ \mu(\omega) + \omega\mu'(\omega) \right\}_{\omega = \omega_o}$$

$$\beta''(\omega_o) = \frac{1}{c} \left\{ 2\mu'(\omega) + \omega\mu''(\omega) \right\}_{\omega = \omega_o} .$$

We can distinguish now the following cases:

First Case

Ionosphere with No Magnetic Field and No Collision

In this case:

$$\beta(\omega_o) = \frac{\omega_o}{c} \mu = \frac{(\omega_o^2 - \omega_p^2)^{\frac{1}{2}}}{c}$$

where

ω_p is the local plasma frequency.

We have furthermore:

$$\beta'(\omega_o) = \frac{\omega_o}{c^2 \beta_o}$$

$$\beta''(\omega_o) = -\frac{\omega_p^2}{c^4 \beta_o^3} .$$

Therefore

$$\beta(\omega) = \beta_o + (\omega - \omega_o)\frac{\omega_o}{c^2\beta^2} - \frac{1}{2} \frac{\omega_p^2}{c^4\beta_o^3} (\omega - \omega_o)^2 + \ldots$$

We see here the $\beta(\omega)$ is not a linear function of ω, and for that the medium is dispersive. Thus Fourier components of a pulse traveling in the medium are displaced from the original mutual phase relationship and the exit waveform is affected by a further degradation, in addition to the one coming from the ray's amplitude response.

Second Case

Ionosphere with Magnetic Field, No Collisions

In this case:

$$\mu^2(\omega) = 1 - \frac{\dfrac{N}{1.24\, f^4 \left(\dfrac{\omega}{2\pi}\right)^2}}{1 - M \pm \sqrt{M^2 + \left(\dfrac{\omega_H}{\omega}\right)^2 \cos^2 \psi}}$$

with symbols as defined in Section 2.0.

The derivatives $\mu'(\omega)$ and $\mu''(\omega)$ have been computed and programmed. From their values, $\beta'(\omega)$ and $\beta''(\omega)$ have been obtained, and finally $\beta(\omega)$ derived.

Third Case

Ionosphere with Magnetic Field and Collisions

$$\mu^2(\omega) = \left[\left(\frac{1}{2} - \frac{A \dfrac{N}{1.24.10^4 \left(\dfrac{\omega}{2\pi}\right)^2}}{2(A^2 + B^2)}\right)^2 + \left(\frac{B \dfrac{N}{1.24.10^4 \left(\dfrac{\omega}{2\pi}\right)^2}}{2(A^2 + B^2)}\right)^2\right]^{\frac{1}{2}} + \frac{1}{2} - \frac{A \dfrac{N}{1.24.10^4 \left(\dfrac{\omega}{2\pi}\right)^2}}{2(A^2 + B^2)}$$

where the symbols have been defined in Section 2.0.

For this case, too, we proceeded to compute $\mu'(\omega)$ and $\mu''(\omega)$ and we went ahead as in the previous case.

4.3 The Wave Polarization

In the cases we are considering in this program, HF sources imbedded in the ionosphere radiate e.m. waves which split in two ionospheric characteristic waves elliptically polarized, in general, and with opposite sense of rotation (ordinary and extraordinary waves).

This phenomenon has an impact on the choice of the most suitable antenna system for satellite-borne terminals and we considered, therefore, interesting to compute the polarization terms of the wave at various points of a ray while performing the tracing.

The polarization term R (usually a complex number) of a wave is defined as

$$R = E_x / E_y$$

where E_x and E_y are the components of the electric vector of the wave, along axes ($\bar{x}$, $\bar{y}$) in the wave front, $\bar{y}$ being in and $\bar{x}$ perpendicular to, the plane containing the imposed magnetic field.

The magneto-ionic theory (Ratcliffe, 1959) indicates that the ellipse of polarization of each wave mode fits into a rectangular "box" with sides parallel to these directions and ratio $|R|$. Ordinary and extraordinary polarization ellipses are related in such a way that one is obtained from the other by reflecting it on the line at 45° with the ($\bar{x}$, $\bar{y}$) axes and reversing the direction of rotation.

The value of Arg R is needed for positioning the ellipse inside the "box" with sides ratio $|R|$.

Our computations started from the magnetoc-ionic formula

$$R = -\frac{j}{Y \cos\psi}\left\{\frac{\frac{1}{2}Y^2\sin^2\psi}{1-X-jZ} \mp \left(\frac{\frac{1}{4}Y^4\sin^4\psi}{(1-X-jZ)^2} + Y^2\cos^2\psi\right)^{\frac{1}{2}}\right\}$$

and we obtained both the expressions of the module and argument of R:

$$|R| \frac{1}{y \cos \Phi} \left[\frac{\frac{1}{4} Y^4 \sin^4 \theta + \left\{ \left[\frac{1}{4} Y^4 \sin^4 \theta + Y^2 \cos^2 \theta (1 - 2X + X^2 - Z^2) \right]^2 + \left[2 Z Y^2 \cos^2 \theta (X - 1) \right]^2 \right\}^{1/2} \mp Y^2 \sin^2 \theta \cos \frac{1}{2} \theta \left\{ \left[\frac{1}{4} Y^4 \sin^4 \theta + Y^2 \cos^2 \theta (1 - 2X + X^2 - Z^2) \right]^2 + \left[2 Z Y^2 \cos^2 \theta (X - 1) \right]^2 \right\}^{1/4}}{1 - 2X + X^2 + Z^2} \right]^{1/2}$$

$$\Phi = \tan^{-1} \frac{-\frac{1}{2} (1 - X) Y^2 \sin^2 \theta \pm \left\{ \left[\frac{1}{4} Y^4 \sin^4 \theta + Y^2 \cos^2 \theta (1 - 2X + X^2 - Z^2) \right]^2 + \left[2Z Y^2 \cos^2 \theta (X - 1) \right]^2 \right\}^{1/4} \left[\cos \frac{1}{2} \theta (1 - X) - Z \sin \frac{1}{2} \theta \right]}{\frac{1}{2} Z Y^2 \sin^2 \theta \mp \left\{ \left[\frac{1}{4} Y^4 \sin^4 \theta + Y^2 \cos^2 \theta (1 - 2X + X^2 - Z^2) \right]^2 + \left[2 Z Y^2 \cos^2 \theta (X - 1) \right]^2 \right\}^{1/4} \left[\sin \frac{1}{2} \theta (1 - X) + Z \cos \frac{1}{2} \theta \right]}$$

These formulas are the least restrictive that can be derived in the the magneto-ionic theory. They are valid in the ionosphere with magnetic field and collision taken into account, and with frequency higher or smaller than plasma frequency and gyrofrequency.

For the frequencies at the upper end of the band we are considering in this program (around 50 mc/s), an analysis of the wave polarization phenomenon can be performed as follows.

Let the z-axis be the direction of propagation and the x-z plane be the plane of the magnetic meridian.

Write the electric vectors in the x and y directions of a completely polarized wave:

$$E_x(0) = a_o e^{i(\omega t + \gamma_a)}$$

$$E_y(0) = b_o e^{i(\omega t + \gamma_b)}$$

$$\omega = 2\pi f.$$

If $\nu/f << 1$ (ν = collision frequency) then on a plane of constant phase the two characteristic waves are in general two ellipses with mutually perpendicular major axes. When entering the ionosphere, the incident wave splits into the two characteristic waves, and with the assumption that $\nu/f << 1$ we can represent this splitting in the following way:

$$E_x(0) = a_o e^{i(\omega t + \gamma_a)} = a_1 e^{i(\omega t + \gamma_1)} + a_2 e^{i(\omega t + \gamma_2)}$$

$$E_y(0) = a_o e^{i(\omega t + \gamma_b)} = b_1 e^{i(\omega t + \gamma_1 + \pi/2)} + a_2 e^{i(\omega t + \gamma_2 + \pi/2)}.$$

From the magneto-ionic theory we know that:

$$\frac{b_1}{a_1} = \eta - \xi; \quad \frac{b_2}{a_2} = \eta + \xi$$

where

$$\xi = \frac{Y_T^2/2\, Y_L}{1 - x}$$

and

$$\eta = \sqrt{1 + \xi^2}$$

As usual

$$x = \left(\frac{\omega_N}{\omega}\right)^2 ,$$

$$y = \omega_H/\omega .$$

Next we define phase constants for the ordinary and the extraordinary rays, namely:

$$K_1(Z) = \frac{\omega}{c} \int_o^z n_1 \, dz = K_1(z)$$

$$K_2(Z) = \frac{\omega}{2} \int_o^z n_2 \, dz = K_2(z)$$

where

n_1 and n_2 are respectively the refractive indices for the ordinary and the extraordinary rays.

Thus at any point z_1 in the ionosphere

$$E_x(z) = a_1 e^{i(\omega t + \gamma_1 - k_1(z)} + a_2 e^{i(\omega t + \gamma_2 - k_2(z)}$$

$$E_y(z) = b_i e^{i(\omega t + \gamma_1 - k_1(z) - \pi/2)} + b_2 e^{i(\omega t + \gamma_2 - k_2(z) + \pi/2)}$$

We can now calculate the necessary parameter to describe the ellipticity and orientation of the polarization ellipses from the following six equations:

$$\tan \gamma_1 = \frac{(\eta + \xi) \sin \Delta a + (b_o/a_o) \cos \Delta b}{(\eta + \xi) \cos \Delta a - (b_o/a_o) \sin \Delta b}$$

$$\tan \gamma_2 = \frac{(\eta - \xi) \sin \Delta a - (b_o/a_o) \cos \Delta b}{(\eta - \xi) \cos \Delta a + (b_o/a_o) \sin \Delta b}$$

$$a_1 = a_o \sin (\Delta a - \gamma_2)/\sin \gamma$$

$$a_2 = a_o \sin (\Delta a - \gamma_1)/\sin \gamma$$

$$b_1 = b_o \sin (\Delta b - \gamma_2)/\sin \gamma$$

$$b_2 = b_o \cos (\Delta b - \gamma_1)/\sin \gamma$$

Δa and Δb are equal to γa and γb originally, while at any later time

$$\Delta a = \tan^{-1} \left[\frac{a_1 \cos (\gamma_1 - k_1 (z)) + a_2 \cos (\gamma_2 - k_2 (z))}{a_1 \sin (\gamma_1 - k_1 (z)) + a_2 \sin (\gamma_2 - k_2 (z))} \right]$$

$$\Delta b = \tan^{-1} \left[\frac{b_1 \cos (\gamma_1 - k_1 (z) - \pi/2) + b_2 \cos (\gamma_2 - k_2 (z) + \pi/2)}{b_1 \sin (\gamma_1 - k_1 (z) - \pi/2) + b_2 \sin (\gamma_2 - k_2 (z) + \pi/2)} \right]$$

Assuming the ellipses travel together through the ionosphere, we calculate the resultant major and minor axes from

$$a = \left\{ a_1^2 + a_2^2 + 2a_1 a_2 \cos (\gamma_1 - \gamma_2 - k_1 (z) + k_2 (z) \right\}^{\frac{1}{2}}$$

$$b = \left\{ b_1^2 + b_2^2 - 2b_1 b_2 \cos (\gamma_1 - \gamma_2 - k_1 (z) + k_2 (z) \right\}^{\frac{1}{2}}$$

The ellipticity is given by

$$p = \tan^{-1} \left\{ \sin^{-1} \left[\frac{\eta (a_1^2 - a_2^2) - \xi [a_1^2 + a_2^2 + 2a_1 a_2 \cos (\gamma_1 - \gamma_2 - k_1 (z) - k_2 (z))]}{0.5 (a_o^2 + b_o^2)} \right] \right\}$$

and the angle between the major axis of the ellipse and the x-axis is given by:

$$\psi = \frac{1}{2} \tan^{-1} \frac{2\eta a_1 a_2 \sin (\gamma_1 - \gamma_2 - k_1 (z) - k_2 (z))}{2a_1 a_2 \cos (\gamma_1 - \gamma_2 - k_1 (z) - k_2 (z)) + \frac{1}{2} (a_1^2 + a_2^2 - b_1^2 - b_2^2)}$$

Computationally, we assign a_o, b_o, γa, γb, η and ξ are calculated at each integration step of the ray-tracing program.

With the initial parameters assigned, and η and ξ calculated at the initial point of the ray trace, we obtain the first set of values for γ_1, γ_2, a_1, a_2, b_1, b_2, ψ and p. At the next point in the ray trace we calculate another set of values for a_{11}, a_{21}, b_{11}, b_{21}, ψ_1, and p_1. The Faraday rotation is given by $\psi_1 - \psi$ and is printed out at every step in the ray trace program.

It should be remembered that this approach is valid only if $\nu/f \ll 1$ and only if the two ellipses travel along the same path. This is true in most of the regions considered in this report for $f \geq 50$ mc/s.

4.4 Phase and Group Velocities along the ray.

4.4.1 Phase and Group Times of Flight ; Equivalent Path Lenghts.

In the Hamiltonian program we have implemented, the variable t represents the time of phase propagation. Therefore, the phase time of flight in a ray is just $\sum_1^n \Delta t_n$ and the equivalent phase path lenght is $c \sum_1^n \Delta t_n$, where Δt_n is the duration of the n^{th} integration step.

The group time of flight is computed according to the formula

$$\sum_1^n \frac{1}{\mu_m} \left(\mu_m + f \frac{\partial \mu_m}{\partial f} \right) \Delta t_n$$

and consequently the equivalent group path lenght is

$$c \sum_{1}^{n} \frac{1}{\mu_n} \left(\mu_n + f \frac{\partial \mu_n}{\partial f}\right) \Delta tn .$$

All these formulas have been introduced in our computer.

4.4.2 The Multipath Structure of the Propagation Modes Considered

The ray tracing we have performed has shown that more than one ray radiated by a source reaches the receiving terminal of the link. Each ray is characterized by its own equivalent group path length. Therefore for each pulse radiated by the source, two and in certain cases three pulses are received, with relative delays in the order of the millisecond, and with waveform deterioration different from a received pulse to another.

The computation of the delays involved in the multipath structure and the evaluation of the expected received waveform are useful data in establishing effective means for facing this type of propagation, encountered in our links. The design of a suitable receiver and the choice of the best waveform to radiate depends on these calculations.

4.5 Sensitivity of the HF Propagation Modes to Refraction and Absorption Effects of Large-Scale Irregularities and Discontinuities

In order to study the sensitivity of the HF propagation modes considered in this program vs. refraction and absorption effects of large-scale irregularities and discontinuities, we have proceeded to the inclusion in our ray tracing computer program of models of irregularities and discontinuities.

The first model computed consists of a sinusoidal ripple imposed in the electron density profile along the direction perpendicular to the magnetic meridian.

Computations, presently underway, will consider various values of the peak of the sinusoidal ripple.

A second model of discontinuity that we have adopted is given in Figure 7 . The model simulates a day-to-night variation of ionospheric electron content. Some preliminary calculations done with this model have shown little effect on the stability of the HF rays considered up until now.

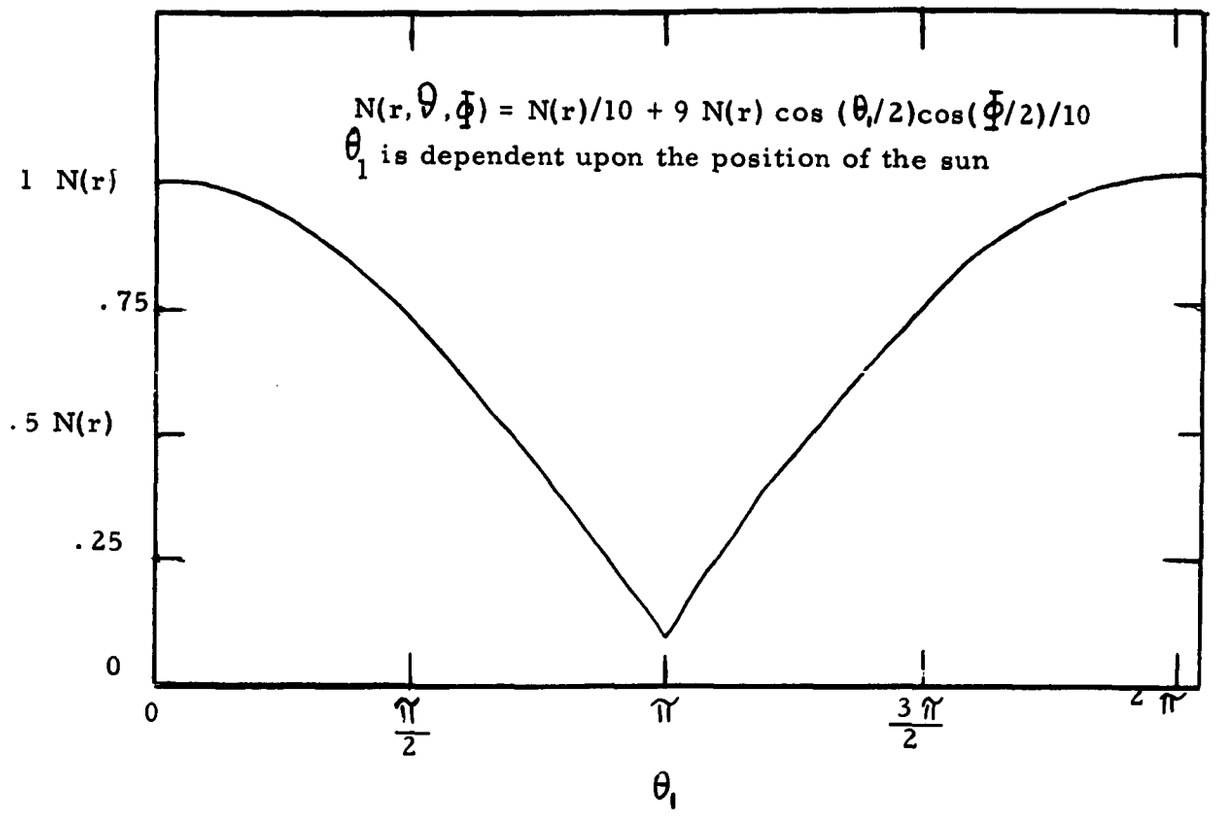

Figure 7 . Model of day-to-night variation of electron density.

A third model that we have developed consists of a mobile spherical disturbance of various miles in diameter representing an excess of electron density in respect of the natural unperturbed three-dimensional profile. In the sphere the variation of electron content from periphery to the center has a gaussian shape. The peak of the electron content excess reaches 10%.

The sphere is computed as approaching a given HF ray path.

At successive time intervals the computer calculates the refraction and absorption effects of the sphere on the HF link. A dynamic picture of the situation is therefore provided. In addition, the computer calculates the equivalent phase path length of the ray, variable vs time. From this curve, the Doppler shift expected at the end of the ray is easily computed.

5.0 THE COMPUTATIONS PERFORMED

5.1 Propagation Modes Underneath the F_2 Layer

The enclosed Table I gives examples of the computations performed in this situation.

The frequencies examined are 40 and 42 mc/s. However, computations have been already performed for frequencies down to 1 mc/s and the possibility of communicating well beyond the line of sight confirmed, up to the lowest limit of the band of our interest.

Case I in Table I shows a ray which performs a circumferential transit from a source at 202.17 Km of altitude in respect of the earth's surface (of radius 6378 Km). The ray makes more than one complete turn around the earth; for simplicity, the table reports R and θ only up to a half complete turn. The ray is trapped between 204 and 54 Km of altitude.

Case 2 shows a ray trapped between 176 Km and 94 Km.

In Case 3 the long-range ray is trapped between 203 and 39 Km; in Case 4 between 175 and 86 Km; in Case 5 between 100 and 166 Km; in Case 6 between 151 and 118 Km; in Case 7 between 149 and 120 Km of altitude.

Computations are presently underway to include the evaluation of the total path losses along these rays. The preliminary results are very encouraging.

5.2 Propagation Across the F_2 Layer

Table II provides examples of computations done up until now in this situation.

Case 1 shows a ray between a source located at 1020 Km and a point at 10 Km of altitude with geocentric angle coverage of about 75°.

Case 2 shows a similar ray between a source at 1006 Km and a point at 10 Km of altitude, with geocentric angle coverage of about 80°.

More computations are underway for this situation, in the search for longer paths.

TABLE I

Rays at various frequencies and with source located underneath the F_2 layer. The angle α is the incidence angle considered in the computations, with zero reference at the vertical. R_o is the distance of the source from the center of the earth; f is the frequency of the source.

CASE 1

f = 42 mc/s

α = 88°

R_o = 6578 km

R_{Km}	θ_{rad}
6580.17	.024864
6575.37	.054687
6547.62	.1040
6508.71	.14801
6453.74	.22163
6435.65	.27121
6432.40	.30104
6434.88	.33089
6445.01	.36564
6480.17	.42482
6548.54	.50300
6570.38	.53749
6581.19	.57721
6576.33	.61698
6536.56	.68104
6466.38	.76419
6452.10	.78886
6434.48	.84343
6432.83	.86830
6449.32	.93782
6491.83	1.0017
6509.19	1.0213
6531.55	1.0457
6582.02	1.1494
6571.96	1.1941

CASE 1, continued

6561.28	1.2139
6526.06	1.2579
6465.16	1.3314
6434.40	1.4106
6433.04	1.4305
6439.29	1.4752
6502.52	1.5787
6553.67	1.6374
6578.56	1.6868
6582.11	1.7117
6575.26	1.7514
6533.16	1.8154
6501.19	1.8495
6473.95	1.8838
6432.99	1.9977
6441.32	2.0474
6446.91	2.0623
6468.71	2.1081
6513.02	2.1556
6547.52	2.1948
6575.93	2.2441
6581.66	2.2739
6581.76	2.2789
6580.61	2.2938
6554.37	2.3531
6503.34	2.4118
6450.85	2.4855
6436.71	2.5252
6432.67	2.5600
6450.23	2.6345
6477.69	2.6789
6493.59	2.6984
6502.19	2.7082
6565.98	2.7866
6581.05	2.8412

CASE 1, continued

R	θ
6579.98	2.8561
6557.13	2.9105
6515.89	2.9594
6455.24	3.0379
6434.24	3.0974
6432.24	3.1223
6434.21	3.1471
6537.80	3.3095

CASE 2

$f = 42$ mc/s

$\alpha = 88°$

$R_o = 6550$ km

R	θ
6551.84	.009880
6553.16	.02965
6549.15	.05931
6533.95	.09871
6504.09	.15272
6483.74	.19699
6473.48	.24142
6472.64	.25626
6504.53	.36474
6521.19	.39418
6541.29	.43349
6553.65	.48780
6549.22	.52239
6531.07	.56671
6503.67	.61579
6473.62	.70451
6472.88	.71934
6486.54	.78847
6505.36	.82782
6539.83	.89164

CASE 2, continued

R	θ
6553.97	.95087
6544.64	1.0002
6517.55	1.0543
6489.43	1.1084
6473.78	1.1676
6473.04	1.1824
6486.72	1.2515
6508.24	1.2958
6524.93	1.3232
6542.06	1.3596
6554.13	1.4140
6536.44	1.4830
6487.65	1.5763
6475.13	1.6208
6473.09	1.6454
6477.42	1.6850
6488.53	1.7195
6500.05	1.7441
6541.85	1.8227
6550.16	1.8473
6554.08	1.8769
6549.69	1.9116
6536.60	1.9461
6499.08	2.0148
6480.77	2.0591
6473.02	2.1085
6478.42	2.1529
6516.02	2.2366
6543.81	2.2709
6551.07	2.3153
6553.87	2.3400
6546.48	2.3845
6496.25	2.4827
6475.69	2.5419

CASE 2, continued

R	θ
6472.82	2.5716
6479.06	2.6209
6505.04	2.6800
6529.81	2.7242
6550.92	2.7784
6553.53	2.8031
6516.57	2.9065
6508.19	2.9212
6486.51	2.9655
6472.84	3.0247

CASE 3

$f = 40$

$\alpha = 88$

$R_o = 6578$

	R	θ
Max.	.65801112E04	.19936876E-01
	.65776100E04	.39871816E-01
	.65704633E04	.59753947E-01
	.65587354E04	.79533906E-01
	.65384971E04	.10407154
	.65145050E04	.12844685
	.64903227E04	.15280969
	.64686494E04	.17728254
	.64505914E04	.20189486
	.64279287E04	.24648566
	.64191818E04	.28133271
Min.	.64178233E04	.30127437
	.64194132E04	.32620146
	.64236619E04	.34612385
	.64325514E04	.37097689
	.64484419E04	.40068734
	.64659811E04	.42531770
	.64918324E04	.45469126
	.65210511E04	.48391777

CASE 3, continued

	R	θ
	.65487047	.51322064
	.65691852E04	.54279999
	.65786970E04	.56764098
Max.	.65810900E04	.58757621
	.65719534E04	.62739948
	.65570105E04	.65211711
	.65361017E04	.67662930
	.65069906E04	.70586299
	.6483421E04	.73025177
	.64556666E04	.76461388
	.64354071E04	.79922593
	.64217378E04	.83899396
Min.	.64181345E04	.87388261
	.64212661	.90378773
	6430.1316	.93363708
	6444.7055	.96337786
	6464.9231	.99295923
	6477.0756	1.0076769
	6499.9177	1.0320976
	6534.0063	1.0661949
	6559.0521	1.0956073
	6575.4073	1.1253054
	6580.6743	1.1452140
Max.	6581.6175	1.1601681
	6575.7821	1.1900494
	6563.1133	1.2148245
	6539.5715	1.2442964
	6510.7199	1.2735412
	6482.3864	1.3028040
	6458.4003	1.3322490
	6439.8918	1.3618827
	6427.0551	1.3916606
	6419.9360	1.4215314
Min.	6418.3770	1.4414705
	6420.0173	1.4663950
	6427.2445	1.4962646

CASE 3, continued

	R	θ
	6440.1891	1.5260404
	6458.8042	1.5556712
	6478.5201	1.5802198
	6506.3702	1.6095041
	6535.5083	1.6387341
	6560.1723	1.6681617
	6576.0317	1.6978727
Max.	6581.7277	1.7277548
	6578.6287	1.7526701
	6565.5230	1.7824435
	6542.9880	1.8119514
	6514.4790	1.8412123
	6481.3310	1.8753482
	6457.5399	1.9048011
	6439.2426	1.9344413
	6426.6197	1.9642238
	6419.7157	1.9940973
Min.	6418.3005	2.0140370
	6420.1204	2.0389611
	6425.9247	2.0638555
	6438.1330	2.0936467
	6456.0212	2.1232991
	6479.4295	2.1527665
	6507.4107	2.182645
	6536.4838	2.2112784
	6560.8370	2.2407189
	6576.2241	2.2704424
Max.	6581.3481	2.3003300
	6577.6965	2.3252420
	6563.8559	2.3549997
	6540.6666	2.3844835
	6511.8857	2.4127318
	6483.3734	2.4429874
	6459.1137	2.4724233
	6443.0560	2.4971005
	64289759	2,5268527
	6420.6070	2.5567093

CASE 3, conintued

	R	θ
Min.	6417.9733	2.5866172
	6421.0816	2.6165228
	6429.9238	2.6463728
	6444.4748	2.6761146
	6464.6703	2.7056970
	6490.1800	2.7350827
	6519.2483	2.7643143
	6547.10018	2.7936079
	6563.0279	2.8231742
	6577.9327	2.8480096
Max.	6580.5984	2.8679436
	6577.3311	2.8928591
	6566.7570	2.9176800
	6549.3116	2.9423183
	6521.8107	3.0008513
	6466.5417	3.0302180
	6445.7883	3.0597835
	6430.6689	3.0895132
	6421.2545	3.1193566
	6418.1621	3.1392895
Min.	6417.5174	3.1542474

CASE 4

$f = 40$

$\alpha = 88$

$R_o = 6550$

	R	θ
	6550	0
	6551.77	.00989
Max.	6552.66	.02474
	6549.45	.04948
	6542.90	.06923
	6530.63	.09384
	6518.74	.11347
	6503.29	.13798
	6486.61	.16746

CASE 4, continued

	R	θ
	6477.71	.18717
	6471.80	.20691
	6465.92	.23164
Min	6464.58	.25144
	6467.13	.28113
	6475.08	.31078
	6488.08	.34034
	6508.17	.37472
	6526.66	.40414
	6544.31	.43858
Max.	6553.15	.48308
	6548.57	.51275
	6533.74	.54726
	6516.00	.57670
	6497.73	.60614
	6482.24	.63564
	6471.31	.66524
	6465.63	.69492
	6464.83	.70976
	6468.29	.74440
	6481.14	.78390
	6496.30	.81341
	6523.71	.85757
	6547.28	.90184
	6553.47	.94140
	6547.60	.97601
	6537.13	1.0006
	6520.00	1.0301
	6492.96	1.0743
	6473.33	1.1186
	6465.02	1.16808
	6470.48	1.2126
	6485.29	1.2520
	6520.02	1.31098

CASE 4, continued

R	θ
6547.67	1.36508
6553.63	1.39970
6548.27	1.4343
6530.05	1.47373
6499.67	1.52278
6473.96	1.5769
6465.06	1.6313
6471.40	1.67585
6497.63	1.73496
6536.28	1.79875
6552.86	1.84811
6553.58	1.86296
6530.95	1.93204
6484.52	2.0105
6467.89	2.05994
6464.98	2.0896
6483.65	2.1687
6520.94	2.2325
6544.54	2.2767
6552.81	2.3312
6522.57	2.4051
6487.24	2.4639
6466.99	2.5232
6464.79	2.5479
6480.81	2.6221
6513.99	2.6810
6543.98	2.73500
6553.04	2.7795
6528.26	2.8536
6494.92	2.9075
6469.83	2.9667
6464.54	3.0063
6490.25	3.1001
6516.98	3.1442
6551.04	3.2181
6552.72	3.2379
6544.82	3.27745

CASE 5

$f = 40$ mc/s

$\alpha = 88°$

$R_o = 6540$ km

R	θ
6540.	0.
6543.32	0.02469
6543.42	0.02963
6528.68	.09375
6500.91	.15274
6484.64	.19706
6479.09	.22667
6478.07	.24644
6485.03	.29582
6513.33	.3647
6533.32	.40895
6543.82	.46324
6509.90	.56667
6492.50	.60602
6479.77	.65534
6478.30	.68004
6485.51	.72941
6502.19	.77372
6525.69	.82286
6542.03	.87213
6544.07	.89683
6524.22	.97078

Case 5 cont'd.

R	θ
6510.01	1.0003
6492.63	1.0396
6479.36	1.0938
6478.47	1.10869
6485.66	1.1630
6504.61	1.2122
6516.49	1.2367
6537.29	1.2859
6543.54	1.3155
6544.23	1.3304
6534.69	1.3797
6515.12	1.4240
6501.07	1.4535
6481.62	1.5126
6478.51	1.5472
6483.11	1.5867
6495.76	1.6261
6518.66	1.6753
6544.18	1.7590
6544.24	1.7639
6526.97	1.8330
6497.00	1.8969
6479.03	1.96396
6478.46	1.98078
6481.92	2.0153

Case 5 cont'd.

R	θ
6493.54	2.0547
6520.72	2.1138
6539.72	2.1630
6544.10	2.1975
6534.80	2.2469
6524.68	2.2715
6508.09	2.3059
6487.79	2.3551
6478.89	2.3995
6478.32	2.4143
6491.54	2.4834
6511.02	2.5277
6536.75	2.5867
6543.55	2.6213
6543.84	2.6312
6528.52	2.6952
6512.30	2.7296
6496.36	2.76407
6483.25	2.80349
6478.1097	2.8479
6488.23	2.90717
6499.70	2.9367
6523.13	2.9858
6533.47	3.0105
6543.48	3.0647

Case 5 cont'd.

R	θ
6533.48	3.11409
6518.43	3.1485
6488.11	3.2173
6477.92	3.2766
6485.63	3.3309

CASE 6

$f = 40_{mcs}$

$\alpha = 88^{\circ}$

$R_0 = 6520$ km

R	θ
6520.	0.
6524.91	.02463
6528.33	.05420
6528.73	.06406
6528.78	.06899
6527.98	.08871
6523.13	.12321
6516.52	.15275
6509.22	.18229
6501.02	.22170
6496.78	.26606
6496.72	.27099
6505.29	.34491
6509.86	.36462

Case 6 cont'd.

R	θ
6519.54	.4040
6528.89	.46805
6529.02	.47791
6524.89	.52228
6512.72	.57644
6504.66	.61092
6499.57	.64047
6496.91	.67991
6499.57	.71934
6509.12	.768607
6521.07	.81784
6528.25	.86218
6529.23	.88190
6526.53	.92183
6517.64	.96566
6509.15	1.0001
6501.91	1.0346
6497.09	1.08389
6497.05	1.0888
6501.19	1.13811
6517.82	1.2119
6522.31	1.2317
6528.40	1.27109
6529.36	1.2957
6522.25	1.3549

Case 6 cont'd.

R	θ
6510.46	1.4041
6505.88	1.4238
6501.19	1.4484
6497.28	1.4878
6497.11	1.4977
6502.91	1.5568
6517.79	1.6208
6523.29	1.6454
6529.38	1.7046
6521.26	1.7687
6509.33	1.8179
6502.93	1.8475
6498.62	1.8770
6497.08	1.9066
6501.95	1.9608
6516.48	2.0248
6524.14	2.0593
6527.82	2.0839
6529.29	2.1135
6524.18	2.1628
6511.62	2.2169
6500.33	2.2712
6496.97	2.3155
6501.03	2.3648
6512.73	2.4189

Case 6 cont'd.

R	θ
6524.92	2.4731
6527.68	2.4929
6529.02	2.5125
6529.11	2.5175
6527.02	2.5520
6514.95	2.6111
6504.42	2.6554
6497.78	2.6997
6496.78	2.7244
6498.36	2.7540
6505.74	2.7983
6519.96	2.8574
6528.03	2.9067
6528.88	2.9264
6522.38	2.9855
6511.85	3.0298
6501.19	3.0791
6496.84	3.1186
6496.59	3.1284
6496.84	3.1432
6508.23	3.2171
6524.27	3.2860
6528.82	3.3304
6528.85	3.3353

CASE 7

$f = 40$ mc/s

$\alpha = 88°$

$R_o = 6515$ km

R	θ
6515.	0.
6520.30	.02462
6526.24	.06897
6527.41	.08868
6524.70	.12811
6520.57	.15275
6514.21	.18229
6504.75	.22661
6498.32	.29068
6500.08	.32519
6506.21	.36460
6515.96	.40892
6525.19	.45817
6527.65	.49761
6522.12	.55182
6517.11	.57644
6506.32	.62568
6499.37	.67495
6498.52	.699606
6500.04	.02918
6505.89	.77352
6510.02	.78829

Case 7 cont'd.

R	θ
6517.77	.82276
6526.24	.87202
6527.86	.90159
6521.95	.96073
6513.55	1.0001
6506.12	1.0346
6498.87	1.0937
6498.65	1.1035
6500.87	1.1430
6508.37	1.1874
6513.83	1.2119
6518.24	1.2317
6525.36	1.2711
6527.99	1.3105
6524.34	1.3549
6516.68	1.3943
6510.04	1.4238
6503.34	1.4582
6498.71	1.5125
6505.68	1.5815
6517.45	1.6356
6524.12	1.6701

Case 7 cont'd.

R	θ
6527.99	1.7194
6521.59	1.7785
6511.96	1.8229
6506.68	1.8474
6505.72	1.8524
6499.62	1.8967
6498.82	1.9115
6498.68	1.9214
6498.72	1.9263

TABLE II

Examples of long-range rays crossing the ionospheric F_2 layer. Symbols as in Table I.

CASE 1

R_o = 6378 km , f = 31.6 mc/s

α = 82.23581°

R_{km}	θ_{rad}
7398.62	1.3261
7285.52	1.2997
7193.06	1.2763
7091.02	1.2481
6996.15	1.2189
6898.47	1.1842
6797.59	1.1384
6699.23	1.0603
6680.57	1.0302
6670,12	1.0051
6660.77	.9697
6650.88	.8376
6649.02	.8028
6648.25	.6510
6648.00	.4991
6647.55	.4384
6646.98	.4030
6646.48	.3827
6645.97	.3675

Case 1 cont'd.

R	θ
6644.79	.3422
6643.00	.3169
6639.63	.2865
6630.17	.2410
6620.98	.2158
6600.07	.1806
6571.34	.1509
6531.90	.1218
6495.27	.0978
6460.37	.0737
6429.05	.0493
6406.76	.0297
6382.40	.0050

CASE 2

R_o = 6378 km

f = 31.6 mc/s

α = 82.23582°

R	θ
7384.10	1.3930
7287.41	1.3703
7194.88	1.3470
7078.70	1.3147
6984.83	1.2854
6888.59	1.2505
6781.89	1.1997

Case 2 cont'd.

R	θ
6686.30	1.1111
6648.71	.8483
6648.20	.6661
6647.99	.4991
6647.55	.4384
6646.98	.4030
6645.97	.3675
6644.48	.3372
6640.95	.2967
6636.27	.2663
6630.17	.2410
6620.98	.2158
6610.45	.1957
6596.06	.1757
6571.34	.1509
6545.99	.1314
6509.94	.1074
6480.93	.0882
6447.38	.0640
6423.25	.0444
6401.58	.0248
6382.40	.0050

5.3 Propagation Modes Above The F_2 Layer

Table III shows some results of our computations for exoionospheric HF links in transversal mode of propagation, with $Y<1$. In computing Table III, we included magnetic field but not collisions in the ionospheric models.

For various geomagnetic latitudes, the expression of μ^2 is computed and surfaces are located where $\mu^2 = 0$ and the ones where $\mu^2 = \pm \infty$.

When the computations presently underway, which include collision, will be completed, we expect to see the conditions $\mu^2 = \pm \infty$ (now at $X = 1 - Y^2$) disappear and a relative maximum of μ^2 appear between the two points which now correspond to $\mu^2 = 0$ ($X = 1 - Y$ and $X = 1 + Y$).

In other words, we expect that a possibility of wave guidance shows up between altitudes now approximately defined by $X = 1 - Y$ and $X = 1 + Y$.

For example, Table III shows that at 3 mc/s, wave guidance should be proved possible between about 1057 Km and about 985 Km, for purely transversal mode of propagation.

Extensive calculations are underway to investigate extension and practicality of this type of guided mode in all the situations from transversal to longitudinal.

TABLE III

Location of Surfaces $X = 1 - Y$, $X = 1 - Y^2$, $X = 1 + Y$ Above F_2 Layer

Geomagnetic Latitude	Frequency Mc/s	Geocentric Altitude (Km) of		
		$1 - Y$	$1 - Y^2$	$1 + Y$
30°	.81	10173.5	9664.5	9084.5
90	.81	9641.5	9269.5	9084.5
150	.81	10173.5	9664.5	9084.5
90	1.24	8550.5	8337.5	8249.5
90	3.00	7435.5	7376.5	7363.5
90	5.00	7123.5	7096.5	7092.5
90	7.50	6957.5	6943.5	6941.5

6.0 SUMMARY

This First Interim Report on the Study of HF Frequencies for Exo- and Endo-Ionospheric Communications illustrates first the main scope of the program, which resides in the search for HF wave guidance modes in the earth's ionosphere. This search is accomplished, having in mind both the requirements of satellite-to-satellite long-range communications, and the requirements of global communications.

The report furnishes details on the analytical tool utilized in the search: a Hamiltonian ray tracing (programmed in an IBM-704 digital computer) which allows the study of ionospheric propagation taking into account nonhomogeneous electron density vs height, nonhomogeneous collision frequency vs height, and the effect of the earth's magnetic field (models spherically symmetric).

The Hamiltonian ray tracing is applied to the search of long-range propagation modes in the ionosphere, between terminals both located above, one above and one below, and both below the F_2 layer.

In addition, the report covers the analysis (that the computer performs while tracing the HF rays) of the basic characteristics of the link.

Total path losses, available bandwidth, multipath structure, sensitivity to large-scale ionospheric irregularities and discontinuities are among the characteristics evaluated.

Examples of the computations performed up until now are provided for the three major cases considered: link above, across, and below the F_2 layer.

7.0 PRELIMINARY CONCLUSIONS

The study performed up until now has shown the existence of HF modes which allow circumferential transits for link terminals located both below the F_2 layer.

Therefore HF communications quite beyond the line of sight appear definitely possible between spacecraft orbiting underneath 350 Km of altitude, up to antipodal positions.

This wave guidance is achievable with carrier frequencies allocated at any point of the band 1 to 50 mc/s. we have examined. Frequencies in the order of 40 to 50 mc/s are, however, preferable from the path losses point of view. Long-range propagation in HF links crossing the F_2 layer has been preliminarily proved by the calculations performed in this program. The rays are of "penetrating Pedersen" type. Path losses computations have not been made final. The data collected until now show, however, higher path losses (due especially to refraction losses) than in the previous case. The possibility of HF propagation beyond line of sight for exoionospheric cases has been preliminarily proved for transversal situations and frequencies higher than the gyrofrequency and for longitudinal situations and frequencies lower than the gyrofrequency. Path losses have not yet been computed in this case.

8.0 RECOMMENDATIONS

Owing to the analytical evidence that this Interim Report already provides about the existence of HF wave guidance modes in the ionosphere, we feel that the organization and coordination of an experiment able to verify the existence of these modes could profitably start very soon.

In fact, at least for the case of HF terminals located below the F_2 layer, we do not expect that the Final Report will change significantly the conclusions already reached, and therefore the analytical data made available already could constitute the base for the experiments' planning.

An ideal experiment would allow an HF propagation survey in the ionosphere, by using specially designed payloads to be flown in satellite programs already underway.

Transmitter and receiver should have available spot frequencies in the band 1 to 50 mc/s; the radiated power should be in the order of about 100 W, the satellites' orbits should be chosen in such a way to allow a wide coverage of link's situations. The superhet receiver should be provided with a matched filter to investigate the multipath structure of the medium; the local oscillator of the receiver should be a high stability one allowing the evaluation of the phase behavior of coherent HF signals received from a suitable HF ground transmitting station. This last feature would allow the collection of data on the structure of ionospheric irregularities and discontinuities which may play an important role in establishing the possibility of having beyond-line-of-sight propagation.

Less than ideal experiments, to be considered specially as a starting point, could utilize the existing NASA-NBS top-side sounder satellite program (which could provide the transmitting terminal of our link) and the AF-Harvard University Space Radio Project (which could provide the receiving terminal of the link). Another experiment, to be performed without the use of satellites, could consist in utilizing the NBS 50 mc/s antenna at Jicamarca, Peru (5×10^4 gain, beam vertically directed, 6 megawatt in the feeder) and in creating an artificial scatterer, for instance with rocket seeding of sodium salt, above it at an altitude of about 125 Km.

We could in this way achieve an effective injection of a powerful 50 mc/s wave in one of the "circumferential transit" modes described in this report.

A ground receiving station, up to antipodal distances, could attempt to receive the trapped 50 mc/s signals by launching, synchronously with Jicamarca, another sodium salt scatterer nearby its vertical. This second scatterer should be

launched in order to "extract" a sizable amount of electromagnetic energy from the ducting.

The cost of this experiment would be limited, inasmuch the Jicamarca station already exists and the technique of injecting by rockets sodium salts in the lower ionosphere has been already fully developed.

A scheme of HF global communications could be explored along this avenue.

9.0 BIBLIOGRAPHY

1. N. C. Gerson, Radio Wave Absorption at Long Distances, pp. 113-125; J. Atm. Terr. Phy., Vol. 23, December 1961, Pergammon Press.

2. Wells, H. W. 1958, Proc. Inst. Radio Eng., 46, 610.

3. Wells, H. W. 1960, AGARDograph 40, Satellites and Problems of Long-Range Detection and Tracking, Pergammon Press, pp. 236.

4. Woyk, E. 1959, J. Atm. Terr. Phys. 16, 124-135.

5. Isted, G. A. 1958, Proc. Inst. Elect. Eng. 105B. Supp. 8-27.

6. Haselgrove, J. The Physics of the Ionosphere, 1955, The Physical Society, London.

7. Hamilton, W. R. 1931, Math. Papers, Vol I., Geometrical Optics, Cambridge University Press.

8. Ratcliffe, J.A., The Magneto-Ionic Theory, 1959, Cambridge University Press.

9. Ratcliffe, J. A., The Physics of the Upper Atmosphere, 1960, Cambridge University Press.

10. Budden, K. G. Radio Waves in the Ionosphere, 1961, Cambridge University Press.

11. Bremmer, H., 1949, Terrestrial Radio Waves, Amsterdam, Elsevier.

12. Makrakis, M.S., J. Atmos. Terr. Phys., 1960, 19, pp 260-271.

13. Lee, C. N., Space-to-Space Propagation Phenomena, Advances Astronautical Sciences, Vol. 3, 1958, Plenum Press, pp. 11-1 to 11-21.

14. Gallet, R. M., and Utlaut, W. F., Evidence of Laminar Nature of the Exosphere. Physical Review Letters, Vol. 6, N. 11, June 1st, 1961, pp. 591-594.

15. Obayashi, T., Journal Rad. Research Lab., Japan 6, 603, 1959.

16. Rawer, K., Radio Propagation Between a Space Vehicle and the Earth in the Presence of the Ionosphere, 1960, Space Research, Interscience Publishers, Inc., New York.

17. Wong, M.S. Ionospheric ray tracing with analog computer, Electromagnetic Wave Propagation, Academic Press, N.Y., 1960.

18. Hildebrand, F.B., An Introduction to Numerical Analysis, McGraw Hill, 1956.

19. A. Ralston and H. Wilf, Mathematical Methods for digital computers, Wiley, 1960.

20. Bennet, Bateman and Milne, Numerical Integrations of Differential Equations, Dover, 1956.

21. Grossi M, Strom K., Strom S. Effects of the ionosphere on HF Radio Astronomy from artificial satellites. SAO Special Report No. 76, 1961.

22. Raytheon Report BR-1095, Propagation of short and medium-short e.m. waves above and in the neighborhood of the ionospheric layer of maximum electron density. 1960.

23. Titheridge, J.E., The effect of collisions on the propagation of radio-waves in the ionosphere, J. Atm. Terr. Physics, 1961, Vol. 22, pp 200-217, Vol. 22, pp. 200-217, Pergamon Press, N.Y.